Biotechnological Journal of Environmental Microorganisms (BJEM)

Biotechnological Journal of Environmental Microorganisms(BJEM) 1(3) 2022 142-154

Grape Seed Extract Loaded Amino Functionalized SBA-15 Mesoporous Silica Nanoparticles as a Potential Drug Delivery System: Antibacterial Activity and Release Kinetics Studies

Mahdi Shahriarinour*[1], Faten Divsar[2] , Zahra Nazari Shad[3]

[1]Department of Microbiology, Rasht Branch, Islamic Azad University, Rasht, Iran
[2]Department of Chemistry, Payame Noor University, PO BOX 19395-3697 Tehran, Iran
[3]Department of Microbiology, Rasht Branch, Islamic Azad University, Rasht, Iran

Received:13 July 2023/ Revised:20 August 2023 /Accepted: 21 August 2023

Abstract

Mesoporous silica nanoparticles (MSNs) are used as efficient carrier candidate for the delivery of the bioactive molecules, proteins, and drugs because of their properties such as safety, stability, biocompatibility, high surface area and controllable pore sizes with the narrow distribution and facile surface modification. MSNs demonstrate high encapsulation capability for both hydrophilic and hydrophobic drugs. In this study, SBA-15 MSN was synthesized by hydrothermal method in acidic media and functionalized by post-grafting method using 3-aminopropyltriethoxysilane. The efficiency of amino functionalized SBA-15 MSN (SBA-15-NH_2) was investigated for the loading and release of grape seed extract (GSE). The disc diffusion assay indicated GSE and GSE loaded on SBA-15-NH_2 (SBA-15-NH_2@GSE) at the concentration of 32 mg/ml extract per disc resulted to in the inhibition zone of 24 mm and 15 mm for *S. aureus* and 22 mm and 13 mm for *E. coli*, respectively. The antibacterial effect improved by increasing concentration of GSE loaded into SBA-15-NH_2 from 2 to 32 mg/ml. These results indicate that SBA-15-NH_2@GSE owns a strong antibacterial potential valuable for the pharmaceutical industry.

Key words: SBA-15-mesoporous silica , Grape seed extract, *E. coli*, *S. aureus*, Antibacterial activity

*Corresponding Author E-mail: mahdi.shahriari@iaurasht.ac.ir

1-Introduction

Grape seed extract (GSE) originated from grape seeds (Vitis vinifera) contains polyphenol-rich compounds such as proanthocyanidins, flavonoids, anthocyanins, and also non-flavonoids. The abundant phenolic chemicals from grape seed are catechins, epicatechin, procyanidin, and some dimmers and trimers (Xia et al. 2010). However, these compounds are available in skin, seed, stem, and pulp of grape. The total phenolic content of GSE varied with cultivar, soil composition, climate, geographic region, and cultivation practices and the history of exposure to infectious agents. Different grape varieties and various extraction methods as well the solvent used in the extraction process may influence phenolic content profiles of GSE (Perumalla and Hettiarachchy 2011). The polyphenol-rich compounds in any formulation of GSE are useful for the cosmetic, culinary, medical and pharmaceutical purposes due to their antioxidant, cardioprotective, hepatoprotective, neuroprotective, anti-diabetic, anti-carcinogen, and anti-aging effect, as well as their antibacterial and anti-inflammatory activity (Nassiri-Asl and Hosseinzadeh 2009). GSE can inhibit the growth of a broad spectrum of Gram-negative and Gram-positive bacteria depended on its concentrations, phenolic content, and tested bacterial species. The GSE is more effective against Gram-positive bacteria than Gram-negative bacteria (Jayaprakasha et al. 2003). Besides bacteria, GSE has also been shown to have inhibitory effects against several clinically important viruses and fungi.

Mesoporous silica nanoparticles (MSNs) are attracting increasing interest for potential biomedical applications because of their tunable pore size, biocompatibility, large specific surface area, adjustable porosity and characterized surface and high chemical and thermal stability (Jafari et al. 2019, Mellaerts et al. 2007). The families of highly ordered mesoporous silicates are MCM-41, SBA-n (n=3, 15, 16) (hexagonal structure) and MCM-48 (cubic structure) with different pore sizes. The discovery of triblock copolymer template SBA-15 was done by Zhao et al., in 1998. The ordered hexagonal pore of mesoporous silica entraps drugs by simple diffusion. The greatly outstanding properties of mesoporous silica make them a capable and broadly used platform for various biomedical purposes, such as bio-imaging for diagnostics, sensing, bio-catalysis, bone repair, scaffold engineering and drug delivery (Divsar et al. 2014, Javanbakht et al. 2009).

MSNs have revolutionized the field of controlled drug delivery systems through their high porosity that can be exploited to confine in its pores a high amount of organic compounds (Doadrio et al. 2015). Moreover, they play an intrinsic role in the stability of the drug by protection from hydrolysis, oxidation or degradation processes by restricting the impact from the surrounding environment (elevated temperature/high humidity) due to the physicochemical stability of the silica matrix. In particular, much effort has been devoted to the design of versatile MSNs for treating diverse pathologies, with special emphasis in cancer treatment (Yang and Yu 2016, Baek et al. 2015, Yang et al. 2014). The interactions between phytochemicals and pristine silica surface are weak, especially hydrogen or van der Waals intermolecular forces. Surface-functionalized mesoporous silica materials have been shown to be perfect space to accommodate molecules of various sizes, shapes, and functionalities. Recently, mesoporous SBA-15 was prepared by the hydrothermal method in the presence of nonionic surfactant (P123) and used as a drug delivery system. SBA-15 is a mesoporous silica sieve based on uniform hexagonal pores with a narrow pore size distribution and a tunable pore diameter of between 5 and 15 nm (Albayati et al. 2019; Shahriarinour et al. 2023). Elbialya et al. combined all the beneficial features of MSNs together with the natural anticancer drug curcumin to develop a polymeric coated curcumin-mesoporous silica nanocarrier for the purpose of cancer diagnosis, therapy and chemoprevention (Elbialy et al. 2020). Chen et al., 2018, constructed multifunctional MSNPs loaded curcumin which was specifically used as a targeted and controlled release drug delivery system. The developed MSNs improve curcumin stability and biocompatibility achieving significant enhancement in their cytotoxicity

against MCF-7 (Chao et al. 2018). Two mesoporous carbons were synthesized via a hydrothermal treatment approach, characterized and evaluated for adsorption properties of berberine hydrochloride and matrine from water (Li et al. 2018). The nanoconfinement effect on polyphenolic extracts prepared from Salvia officinalis L. and Thymus serpyllum L. into the mesopores of silica and titania nanomaterials was studied on their radical scavenging capacity and antimicrobial potential. The results evidenced the role of mesoporous inorganic materials, silica, and titania as support for polyphenolic extracts on improving the natural compounds stability (Brezoiu et al. 2020; Shahriarinour et al. 2021). In our previous study, thymol loaded SBA-15 mesoporous silica nanoparticles demonstrated high antibacterial activity against gram-positive and gram-negative pathogenic bacteria (Shahriarinour et al. 2019).

However, there are limited papers on the antibacterial study of herbal extract loaded mesoporous. As far as it is known, it is among the pioneer studies concerning the antibacterial study of the SBA-15-NH_2@GSE. Herein, we synthesized SBA-15 MSN and then amine functionalized it using 3-amino propyltriethoxysilane. After that, GSE was loaded into the modified mesoporous and subsequently was evaluated for the controlled release. Finally, the antibacterial property of GSE, SBA-15-NH_2, and SBA-15-NH_2@GSE was characterized against pathogenic bacteria of *S. aureus* and *E. coli*.

2.Material and Methods

2.1. Chemicals and reagents

Pure analytical grade materials, Tetraethyl orthosilicate (TEOS) (99.9%), (3-Aminopropyl) triethoxysilane (APTES) (98%), toluene (99.99%), HCl (37%), EtOH (99.9%), acetone (99.9%), diethyl ether (99.9%), Mannitol salt agar (MSA) and Eosin methylene blue (EMB) were purchased from Merck (Darmstadt, Germany). Pluronic triblock copolymer P123 was prepared from Aldrich. Muller-Hinton Agar and Muller-Hinton Broth were purchased from Quelab (UK) and Merck (Germany), respectively. Grape seed extract was prepared by Zardband Pharmaceuticals Company (Tehran, Iran). *Staphylococcus aureus* PTCC1113 and *Escherichia coli* ATCC 25922 were supplied by Iranian Research Organization for Science and Technology (IROST). All bacteria strains were maintained stock at -80C. Blank Disc was purchased from Padtanteb (Iran).

2.2. Instruments and equipment

The patterns of powder X-ray diffraction of the samples were acquired using X-ray diffractometer (X'Pert Pro MPD, PANalytical) using Cu Kα radiation (λ= 1.54Å) in the range 2θ=0.88-10°. Philips model XL30 with a field emission at the voltage of 15KV was utilized to record scanning electron microscopy (SEM) images. FT-IR spectra were documented using the TENSOR 27 (Germany) spectrometer in the gamut of 400-4000 cm-1. The UV-Vis diffused reflectance spectra (UV-Vis DRS) were gained using UV-Vis Scinco 4100 spectrometer with an integrating sphere reflectance accessory. Nitrogen adsorption/desorption isothermal, parameters of Brunauer-Emmett-Teller and Joyner Halenda were obtained by ASAP 2020 at 77K. The UV/Vis absorption spectra were calculated by a Shimadzu UV-1600 PC spectrophotometer.

2.3. Synthesis of SBA-15 MSN.

The synthesis of the SBA-15 MSN was performed according to the previously reported method (Javanbakht et al. 2009). Briefly, 4 g of surfactant P123 was dissolved in a mixture of 20 ml of HCl (37%) and 104 ml deionized water at 40°C for 2h. TEOS was added drop-by-drop for several minutes and kept at 40 °C for 24h. After, the mixture heated at 90 °C for 24h. Finally, the solid phase was recovered by filtration and washed with deionized water, diethylether, and acetone. The product was dried at 100 °C and calcined at 600 °C for 6h.

2.4. Synthesis Amine Functionalized SBA-15 (SBA-15-NH_2).

This step was performed according to post synthesis method (Song et al. 2005) . SBA-15 (1.0g) was suspended in anhydrous toluene and then APTES (4 mmol) was added drop-by-drop over several minutes. The suspension was refluxed for 24 h. Afterward, the solid phase was recovered by filtration and washed with toluene. The product was dried under a high vacuum.

Biotechnological Journal of Environmental Microorganisms (BJEM)

Biotechnological Journal of Environmental Microorganisms(BJEM) 1(3) 2022 142-154

2.5.GSE loading

Typically, 80 mg of SBA-15-NH_2 and 80 mg GSE was suspended in 10 mL solution of EtOH (30%). Then the mixtures were stirred at room temperature for 72 h and then kept in a refrigerator for 24 h. The drug-loading SBA-15-NH_2 powder was recovered by vacuum filtration and dried at room temperature. Then, it was analyzed for GSE content at 340 nm using UV-Vis spectrometer. Adsorption of GSE using 1:1 ratio changed SBA-15-NH_2 to red powder. The efficiency of encapsulation (EE) and capacity of loading (LC) were then determined by following equations:

$$\%EE = \frac{\text{weight of GSE in SBA}-15-NH2}{\text{weight of GSE used}} \times 100 \quad (1)$$

$$\%LC = \frac{\text{weight of GSE in SBA}-15-NH2}{\text{weight of GSE in SBA}-\frac{15}{NH_2}+\text{Weight of SBA}-15-NH2} \times 100 \quad (2)$$

The supernatant was analyzed by UV-Vis spectrophotometry at wavelength 340 nm to determine the polyphenol loaded within the SBA-15-NH_2 matrix.

2.6. In Vitro Release of GSE.

The release profile of GSE was studied by 10 mg SBA-15-NH_2@GSE in a dialysis bag (MWCO=14000 Da). The dialysis bag was immersed in 100 mL phosphate buffer saline (PBS, 0.01M, pH=7.4) while stirring at 37 °C and 150 rpm. At certain time, 2 mL of samples were taken for further analysis. The release of GSE was measured by UV-Vis method at the wavelength of 340 nm. Computation of the corrected concentration of the released GSE is based on the following equation:

$$C_c = C_t + \frac{\nu}{V}\sum_0^{t-1} C_t \quad (3)$$

Where Cc represent the corrected concentration at time, Ct represent the apparent concentration at times, ν represent the volume of samples taken, and v represent the total volume of released fluid.

2.7. Disc Diffusion Method.

The disc diffusion method was performed by paper discs containing 20 µL of (32mg/ml) formulations of antimicrobial susceptibility testing (Nahaei et al. 2016; Shahriarinour and Divsar 2023). Inoculation plates were swabbed by dipping a sterile cotton-wool into the bacterial suspension (approximately 0.5 McFarland standards). Excess bacterial suspension was cleaned off by tapping the swab against the side of the container. Then, inoculation was carried out over all the surface of the plate. The Discs containing of GSE, SBA-15-NH_2@GSE, and SBA-15-NH_2 were placed on the surface of the agar. The plates were incubated at 37°C for 72h then the zones of growth inhibition were measured around discs in the millimeter. The experiment was repeated three times independently.

2.8.Minimum Inhibition Concentration Determination (MIC).

Minimum Inhibition Concentration "MIC" is the minimum antimicrobial concentration agent that stops the observable growth of bacteria. In this investigation, MIC was calculated by broth macro dilution tube method (Holla et al. 2012). A tube containing 1 mL of 32 to 0.32µg /ml of antimicrobial agents was prepared. Then, 1 mL of bacterial suspension (0.5 McFarland standard) in the Mueller Hinton Broth was inoculated into the tubes and were incubated at 37oC overnight. MIC was determined as the minimum concentration of GSE that repressed growth of *E. coli* ATCC 25922 and *S. aureus* PTCC1113.

2.9. Minimum Bactericidal Concentration Determination (MBC).

Minimum Bactericidal Concentration "MBC" is a minimum concentration that kill bateria (Omara et al. 2017). This step was specified by sub-culturing 50 µL of each test tube showing no apparent growth. The minimum concentration of a test substance showing no evident growth of sub culturing was taken at MBC.

3. Results and discussion

The strategy developed by Song et al. 2005 was adapted by modification of few parameters to obtained amine functionalized silica mesoporous nanoparticles. Fig 1. shows a schematic view of the

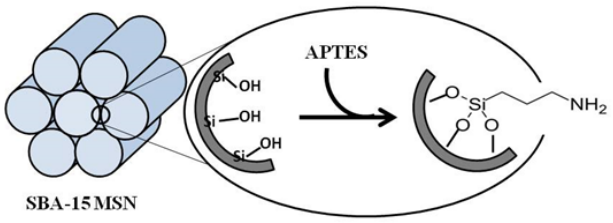

Fig. 1. Schematic illustration of the APTES binding mechanism to silanol groups of the SBA-15 cylindrical mesopores.

SBA-15 MSN and the presence of silanol groups. Amine functionation was done using covalent binding of APTES.

3.1. X-ray Diffraction Spectra and Scanning Electron Microscopy Image.

The low-angle XRD array of SBA-15-NH_2 is illustrated in Figure 2. Three peaks can be observed for SBA-15-NH_2 indexed as (100), (110) and (200) suggests the well ordered two-dimension (2D) hexagonal meso structure, which is approved in other reports (Yang et al. 2003). The XRD spectra of SBA-15-NH_2 detected at 1.148°, 2.13°, and 2.794° are attributed to the (100), (110) and (200) crystallographic planes.

The particle size and morphology of the SBA-15-NH_2 are shown in scanning electron microscopy (SEM) image (Figure 3). It is clear that all the particles are cylindrical shape and uniform in size. These results illustrate that the modification of the SBA-15 did not affect the morphology of the materials.

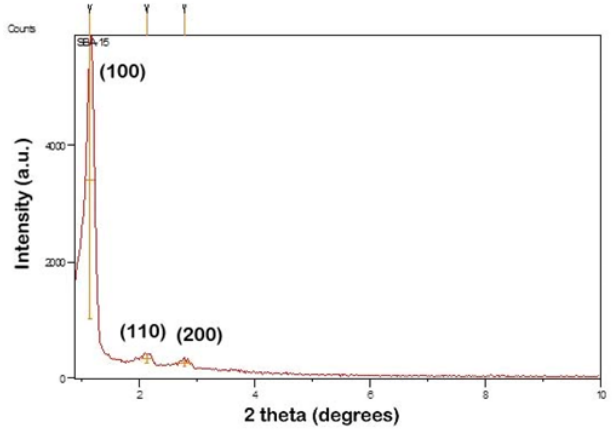

Fig. 2. The low-angle XRD patterns of SBA-15-NH_2.

3.2. Fourier Transform Infrared Spectroscopy Analysis.

FT-IR spectra of SBA-15-NH_2, GSE, and GSE loading on SBA-15-NH_2 are shown in Figure 4 A, B and C, respectively. The band of 464.81cm^{-1} of part A and 484.81cm^{-1} of part C are appointed to the Si-O-Si bending mode (Bagherzadeh et al. 2018). The bonds between 1645.17 to 1550.66 cm^{-1} are shown N-H bending, 3100-3400cm^{-1} represent N-H stretching vibration (overlap with O-H) and 1442.66-1519.80 cm^{-1} C-N denote through amino group of SBA-15-NH_2 (Figure 4A). The absorbance peaks at 796.55 cm^{-1} and 1081.99 cm^{-1} are because of Si-O-Si symmetric and asymmetric stretching vibration of the silica group (Figure 4C). The peaks of Si-OH (silanol) that appeared at 3745 cm^{-1} are also observed in the spectra of SBA-15-NH_2 and SBA-15-NH_2@ GSE (Figure 4A and Figure 4C). The FT-IR spectra of GSE and GSE@SBA-15-NH_2 are shown in Figure 4B and Figure 4C. These peaks at 721.11, 838.98, and 1043.42 cm^{-1} corroborate C-H bending vibration, C-H out of the plane and C-C stretching aromatic in the ring from GSE. The bonds spanning 2883.38 and 2935.46 cm^{-1} for GSE show CH2 stretching vibration both symmetric and asymmetric, respectively. The spectra for O-H detected peaks in the 3200-3600 cm^{-1} corresponded to the hydroxyl stretching of the hydrogen-bonded internal OH at phenol group. The peaks at 1232.43, 1386.72, 1550.66 and 1641.31 cm^{-1} indicate C-O stretching vibration at the phenol ring, C-O-H bending and C=C stretching vibration at the phenolic ring, respectively (Figure 4B). The peaks at SBA-15-NH_2@ GSE (Figure 4C) confirm loading GSE on SBA-15-NH_2. The bonds of GSE at 1390.58, 1413.72, 1550.66, 1641, 2893.02, 3072.39, and 3365.55 cm^{-1} are also observed in the spectra of SBA-15-NH_2@GSE. These data demonstrate the loading of GSE to SBA-15-NH_2. The peaks shift toward higher position about 1 cm^{-1} after forming SBA-15-NH_2@GSE. The peaks at 484.81, 796.55, and 1081.99 cm^{-1} show Si-O-Si bending, symmetric, and asymmetric stretching vibration at SBA-15-NH_2 (Figure 4C).

3.3. UV-Vis Diffused Reflectance Spectroscopy.

Figure 5 shows the UV-Vis DRS spectra of SBA-15-NH_2 (A) and SBA-15-NH_2@GSE (B) in the range 300-1000 nm. The UV-Vis DRS spectra show sharp bands at 300 nm for SBA-15-NH_2 and two broad bonds 350 nm and 400 nm for SBA-15-NH_2@GSE. The broad peak at 400 nm depicts loading GSE on SBA-15-NH_2 which is the characteristic bands of GSE (Yarovaya et al. 2019).

3.4. BET and BJH Analysis.

The N2 adsorption-desorption isotherms were used to determine the specific surface areas from the standard BET equation at the relative pressure (p/p0) from 0.0 to 0.99 and the cross-sectional area of nitrogen molecule of 0.162 nm2.

Biotechnological Journal of Environmental Microorganisms (BJEM)

Biotechnological Journal of Environmental Microorganisms(BJEM) 1(3) 2022 142-154

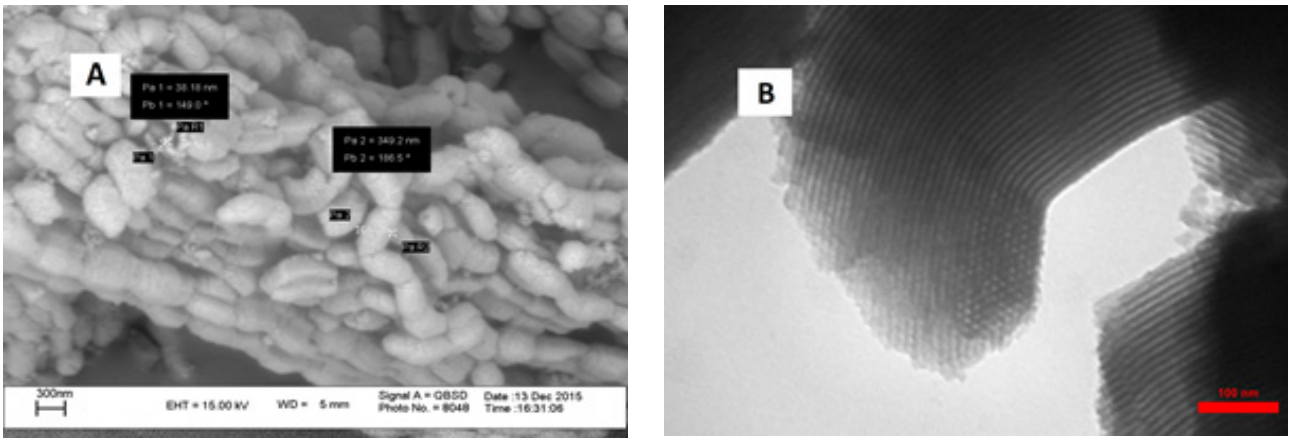

Fig. 3. (A) SEM and (B) TEM image of SBA-15-NH_2.

Figures 6 A1 and A2 show the N2 isotherm of SBA-15-NH_2, and SBA-15-NH_2@GSE. Figures 6 B1 and B2 exhibit pore size distribution using Barrett Joynerand Halenda (BJH) method. All samples yield IV type of isotherm with H1 hysteresis loop. This well-defined hysteresis loop of H1 type rendering to the IUPAC classification shows parallel branches of adsorption and desorption (Goscianska et al. 2017, Ziarani et al, 2012). The BET surface area (a s, BET), average pore diameters (dp), total pore volume (Vtot), and volume of gas adsorbed at STP (Vm) were obtained by Brunauer, Emmett and Teller (BET) method for two samples as shown at Table 1. The BET model was measured surface area (as, BET) values of 180.78 and 0.3824 m2.g-1 for SBA-15-NH_2 and SBA-15-NH_2@GSE. The values of Vtot and Vm for SBA-15-NH_2@GSE were smaller than those for SBA-15-NH_2. The dp was measured 8.6087 and 5.8899 nm for SBA-15-NH_2 and SBA-15-NH_2@GSE, respectively. As a result, average pore diameters decreased about 2.7 nm after loading GSE on SBA-15-NH_2.These results confirm the encapsulation of GSE into all channels of the SBA-15-NH_2 pores. The BET t-plot was shown for SBA-15-NH_2 and SBA-15-NH_2@GSE at Figure 6 C1 and C2. The Barrett–Joyner-Halenda (BJH) models calculated pore size distribution curves, area pore (ap) mean volume of the pore (Vp) and radius peak (rp). The value of Vp was decreased from 0.2573 to 0.000855 for SBA-15-NH_2 and SBA-15-NH_2@GSE. The surface area pores (ap) were obtained by the BHJ method of SBA-15-NH_2@GSE smaller than SBA-15-NH_2, therefore pores are full of GSE. The rp of SBA-15-NH_2@GSE is slightly smaller than that SBA-15-NH_2, since the pores encapsulation of GSE can cause decrease in ap, Vp and rp. The rp reduced from 4.03 nm to 2.71 nm.

Table. 1. The structure parameter of SBA-15-NH_2 and SAB-15-NH_2@GSE was synthesized.

Formulation	$a_{s,\ BET}$ ($m^2.g^{-1}$)	V_{tot} ($cm^3.g^{-1}$)	d_p (nm)	a_p ($m^2.g^{-1}$)	V_p ($cm^3.g^{-1}$)	r_p (nm)
SBA-15-NH_2	180.78	0.2662	8.6087	0.1807	0.2573	4.03
SBA-15-NH_2 @GSE	0.3824	0.00087	5.8899	0.00047	0.000855	2.71

BET surface area (a_s) calculated in the range of relative pressure (p/p_0) 0.0 to 0.99; d_p =average pore diameter; V_{tot} = total pore volumes measured at (p/p_0) 0.988; V_p = mean volume of the pores; a_p = surface of pores, r_p= radius pores.

3.5. Loading and Release of GSE.

Linear regression analysis of total soluble phenolic content was obtained at concentrations of 0.032 - 32 mg/ml in distilled water. The equation regarding the calculating calibration curve was termed as: y=0.1304 x + 0.0526

Where y denote the absorbance and x denote the equivalent content of polyphenol compound at the wavelength of 340 nm (Yarovaya et al. 2019). The GSE was loaded into SBA-15-NH_2 using 32 mg/ml of extract and then LC and EE were obtained. The values of LC and EE are 87.62% and 97.21%, respectively. These results indicated that the high amount of GSE was loaded in the channels of SBA-15-NH_2. Afterward, the profile release of GSE was acquired at 1, 2, 3, 4, 5, 6, 12, 18, 24, 30, 36, 40, 46, 52, 62, 72 and 82 hours from SBA-15-NH_2@GSE. The release rate of GSE from SBA-15-NH_2@GSE was about 7.2% at first hour. The releasing percentage augmented to 97.5% at 82h. In general, the release of GSE is slow for SBA-15-NH_2@GSE at certain times. The release rate of GSE elevated until 46 h, after that the rate of release became slower. The release profile of GSE is observed at Figure 7.

3.6. Kinetic Modeling

The linear form of the zero, first and second order kinetic models of GSE biodegradation are written in equation (1) to (3), respectively, as:

$$C = C_0 - kt \quad (1)$$

$$-\ln(C/C_0) = k_1 t \quad (2)$$

$$(1/C) - (1/C_0) = k_2 t \quad (3)$$

where, C_0 and C (mg/mL) are the initial and final concentrations of the drug, respectively. k1 (1/day) and k_2 (mL/mg day) are the rate constants of the first and second order kinetic models, respectively. The plot $-\mathrm{Ln}(C_0/C)$ versus t is respected to give a straight line if first order kinetics is applicable. While, the plot $[(1/C) - (1/C_0)]$ versus t should give a straight line if second order kinetics are usable. The k_0, k_1 and k_2 values can be determined from the slope of the plots, respectively. Table 2 shows the kinetic constants for GSE release from the SBA-15-NH_2 @ GSE. The R_2 values demonstrate that the release profile is based on the zero order kinetic.

3.7. Thermodynamic Study

The Eyring–Polanyi equation can describe the variance of the rate of a chemical process with temperature. The linear form of this equation is:

$$\mathrm{Ln}[(k.h)/(KBT)] = -(\Delta H/R)1/T + \Delta S/R$$

where, k is rate constant, KB is Boltzmann constant = 1.38066 × 10−23 J/K, R is universal gas constant = 8.31441 J/mol K, h is Planck constant = 6.6262 × 10−34 J s, ΔH (J/mol) and ΔS (J/mol K) are changes of enthalpy and entropy, respectively. ΔH and ΔS can be obtained from the slope and intercept of this equation.

On the other hand, the change of Gibbs free energy (ΔG) of process can be obtained after determination of ΔH and ΔS values from the Van't Hoff equation: $\Delta G = \Delta H - T\Delta S$

The final concentration of GSE (C_0= 32 mg/ml) was determined at pH = 7.4 and different temperatures. The k1values were determined about 0.0345, 0.0258 and 0.0234 1/hour (by treatment SBA-15-

Table. 2. The kinetic constants of release GSE from the SBA-15-NH2 @ GSE by different treatments.

	y=ax+b	k	R^2
Zero order	y = 3.9526x + 13.327	3.9526	0.9046
First order	y = -0.1097x + 1.8721	0.1097	0.6707
Second order	y = -0.0044x + 0.0713	0.0044	0.3764

Biotechnological Journal of Environmental Microorganisms (BJEM)

Biotechnological Journal of Environmental Microorganisms(BJEM) 1(3) 2022 142-154

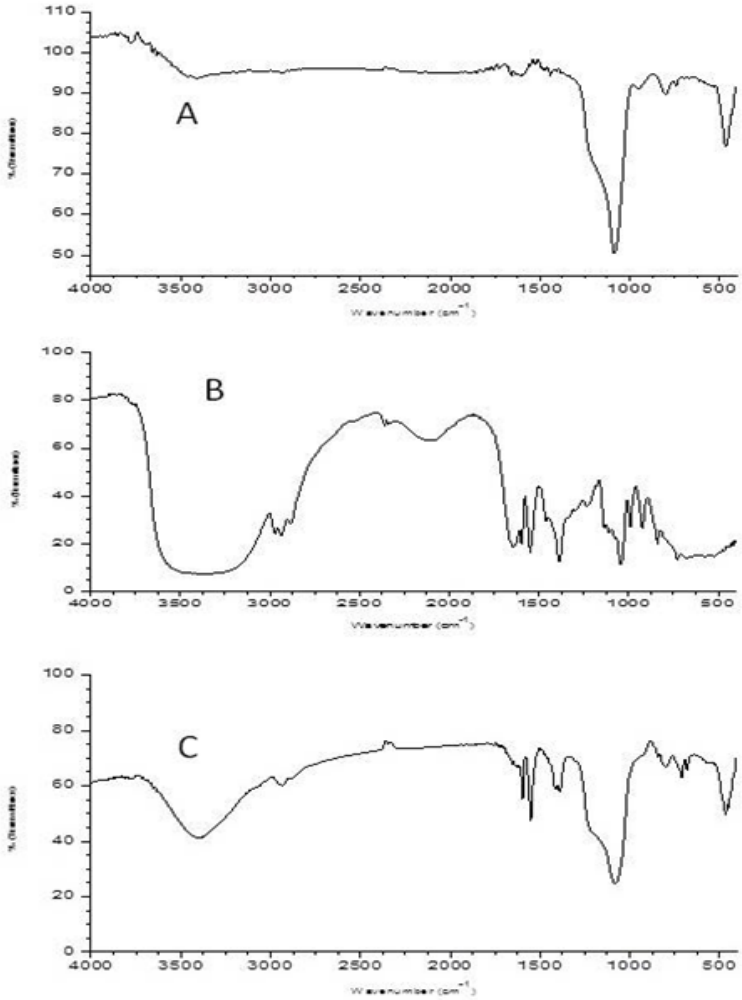

Fig. 4. FT-IR spectra of SBA-15-NH_2 (A), GSE (B), and SBA-15-NH_2@ GSE (C).

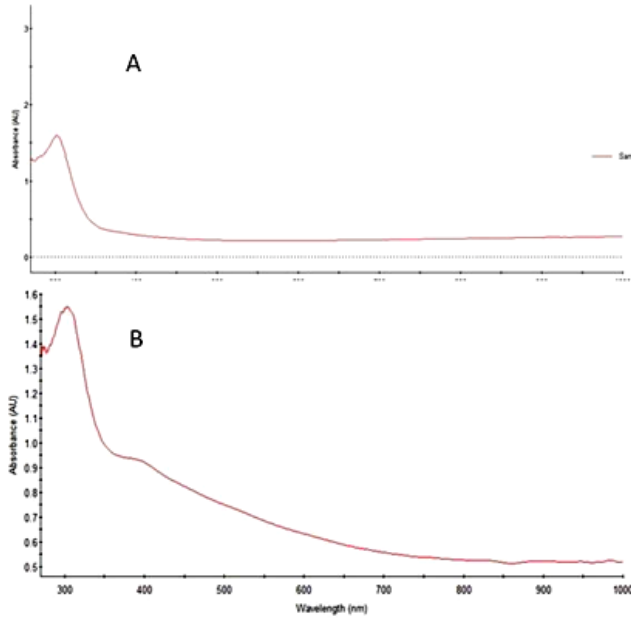

Fig. 5. DRS spectra of SBA-15-NH_2 (A) and SBA-15-NH_2@ GSE (B).

NH_2 @ GSE, pH = 7.4) during 18 h at 288, 298 and 308 K, respectively. According to Fig. 8, ΔH and ΔS values of this process were obtained +243.97 kJ/mol and −4.79 kJ/mol K, respectively. The positive ΔH value shows the endothermic character of the process and the negative value of ΔS shows decreasing disorder at the interface between GSE and carrier. On this basis, ΔG values at 288, 298 and 308 K were determined + 1624.74, +1672.68 and+ 1720.63 kJ/mol, respectively. The positive value of ΔG confirms the non-spontaneous process, thermodynamically.

3.8. Antibacterial Activity.

The antibacterial properties of GSE, SBA-15-NH_2, and SBA-15-NH_2@GSE were measured by disc diffusion method using *E. coli* and *S. aureus*, as pathogenic bacteria. All of the obtained results are summarized in Table 2. SBA-15-NH_2 showed no antibacterial property versus gram-negative (*E. coli*) and gram-positive (*S. aureus*). GSE showed antibacterial properties for *E. coli* and *S. aureus* at various concentrations from 2 to 32 mg/ml were incubated at 37°C for 72 h (Table 2). The maximum zone of growth inhibition was observed 22 mm and 24 mm for as *E. coli* and *S. aureus* with the highest concentration (30 mg/ml) of GSE. The lowest concentration (2 mg/ml) of GSE was shown 11 mm and 12 mm zone of growth inhibition for gram-negative and gram-positive pathogen bacteria, respectively. Even the SBA-15-NH_2 loaded with various concentrations of GSE (2 to 32 mg/ml) show the antibacterial effect for *E. coli* and *S. aureus*. The SBA-15-NH_2 containing GSE indicated the highest area of growth suppression against *S. aureus* around 15 mm (32 mg/ml of GSE) and 7 mm (2 mg/ml of GSE). However, the lowest inhibition activity was shown against *E. coli* about 6 mm and 13 mm for the 2 and 32 mg/ml of GSE solution, respectively.

The antibacterial feature of SBA-15-NH_2@GSE was subordinate in comparison to pure extract. However, SBA-15-NH_2 lacks antibacterial effect in both bacteria. The Figures 9 and 10 show zone of growth inhibition of the GSE (A), SBA-15-NH_2 (B), and SBA-15-NH_2@GSE (C) from 72 h for *S. aureus* and *E. coli*.

Table 3 show that the intense antibacterial effect is elevated with the concentration of GSE or SBA-15-NH_2@GSE for gram-positive and gram-negative bacteria. The highest concentration of GSE and SBA-15-NH_2@GSE showed a high inhibition effect against *S. aureus* compared to the *E. coli*. The area of growth suppression of SBA-15-NH_2@ GSE increased from 24h to 72h for *S. aureus* and *E. coli*. These data depict that GSE released through pores of SBA-15-NH_2 after 24 h until 48 h noticeably. The curves are shown in the ure 11A and B.

4. Conclusion

This study evaluated the bactericidal efficacy of pure GSE, SBA-15-NH_2 and SBA-15-NH2@ GSE against *E. coli* and S. aurous. These data demonstrate that the mesopours silica SBA-15-NH_2 can be an excellent carrier for GSE. The GSE adsorption into the SBA-15-NH_2 improved through hydrogen bond between phenol groups of GSE and amino groups of SBA-15-NH_2. The release profile of GSE from SBA-15-NH_2@GSE was studied over a 82 h period at 37 ºC. The highest antibacterial effect was observed for GSE and SBA-15-NH_2@GSE at concentration 32 mg/ml of the extract against *S. aureus* bacteria.

Acknowledgments

The authors are humbly thankful to Rasht Branch, Islamic Azad University for supporting this study.

Table. 3. The antibacterial activity of the GSE, SBA-15-NH_2, and SBA-15-NH_2@GSE against *S. aureus* and *E. coli* incubated at 37°C for 72h.

Formulations	*S. aureus*					*E. coli*				
	Concentration (mg/ml)									
	2	4	8	16	32	2	4	8	16	32
	Zone of inhibition (mm)									
GSE	12	14	17	22	24	11	14	16	19	22
SBA-15-NH_2 @GSE	7	9	11	13	15	6	8	10	11	13
SBA-15-NH_2	-	-	-	-	-	-	-	-	-	-

(-)Non antibacterial effect

Biotechnological Journal of Environmental Microorganisms (BJEM)

Biotechnological Journal of Environmental Microorganisms(BJEM) 1(3) 2022 142-154

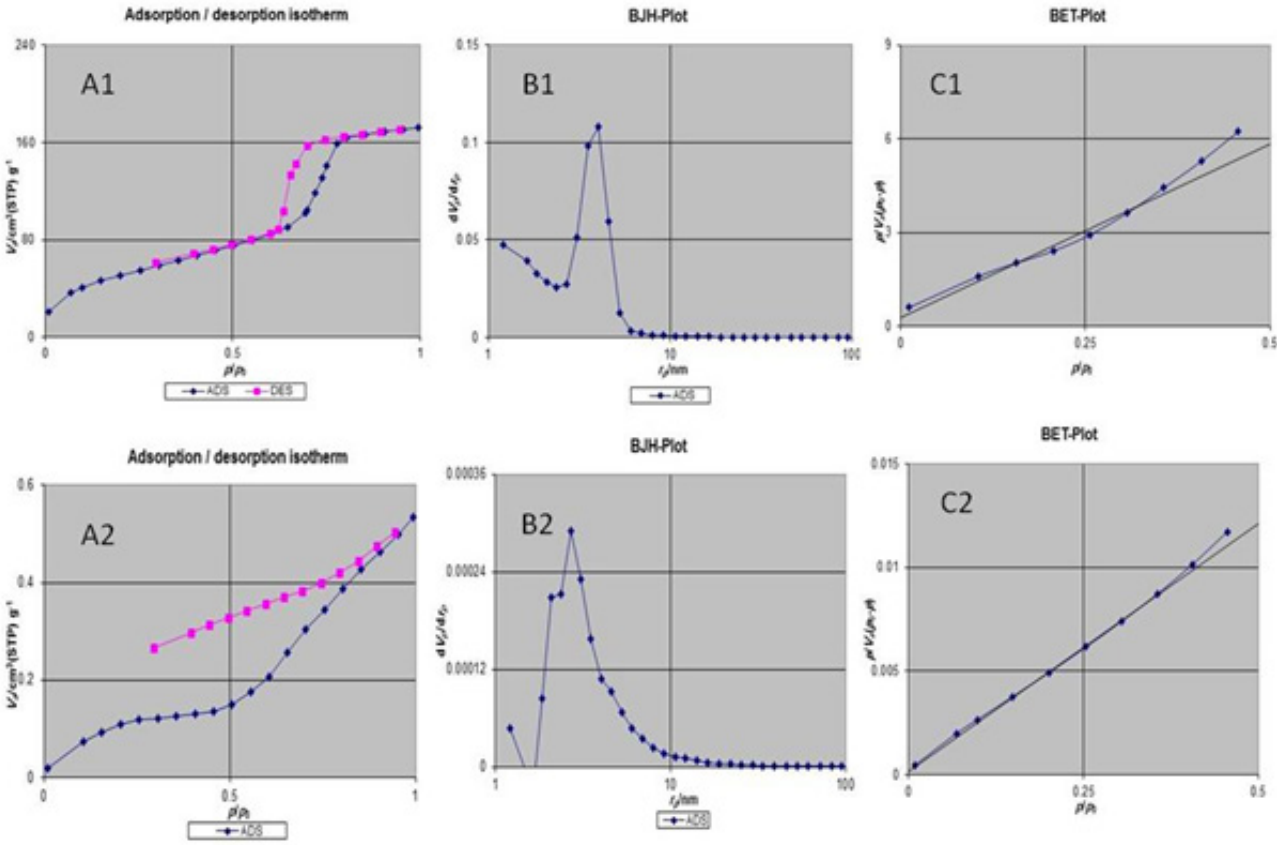

Fig. 6. N_2 adsorption-desorption isotherms measured at 77 K (A1, A2); their pore size distribution curve (B1, B2) and BET t-plot (C1, C2) of SBA-15-NH_2 and SBA-15-NH_2@ GSE, respectively.

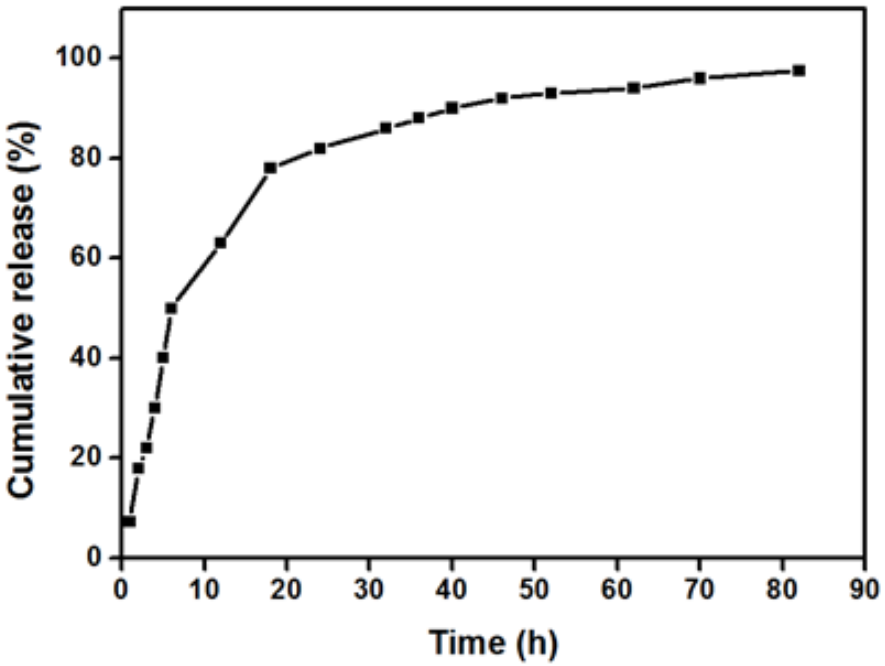

Fig. 7. Cumulative release (%) of GSE form SBA-15-NH_2 @ GSE at PBS (pH=7.4).

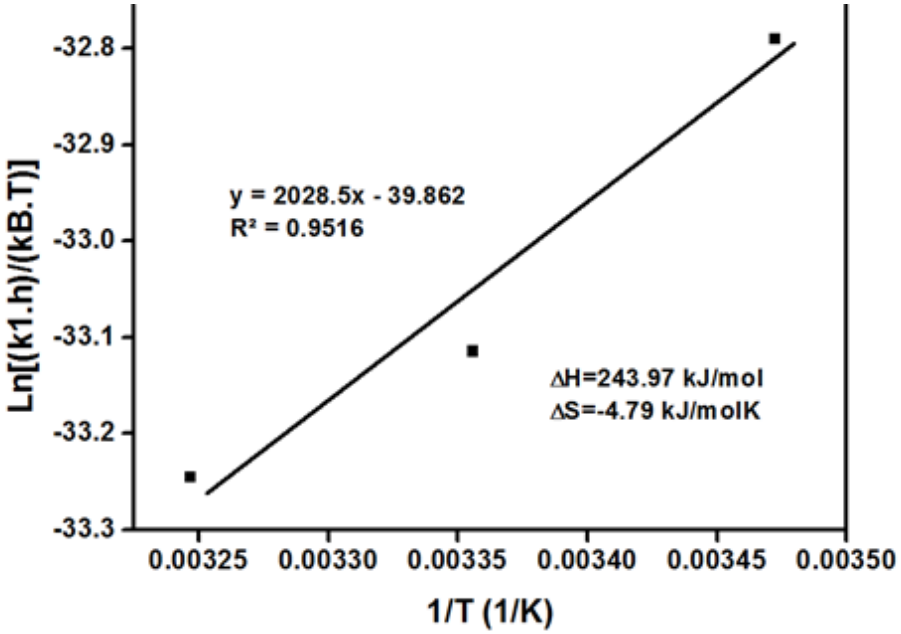

Fig. 8. Eyring–Polanyi model for degeradation of alprazolam at different temperatures and pH = 7.4 during 18 h to determine thermodynamic parameters.

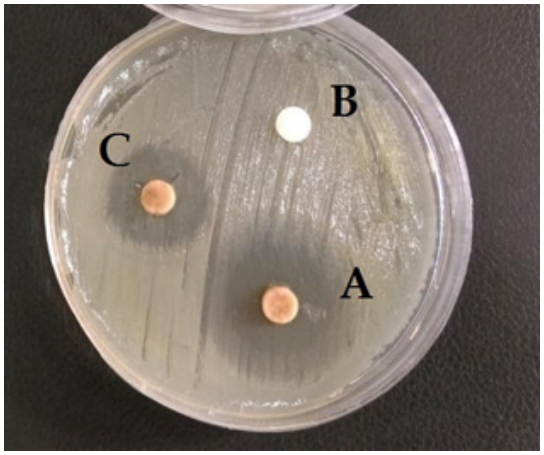

Fig. 9. Inhibition zones of GSE (A), SBA-15-NH_2 (B), and SBA-15-NH_2@ GSE (C) on *S. aureus*.

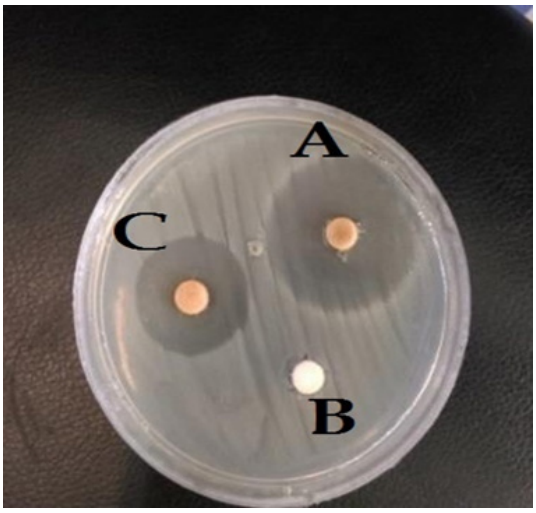

Fig. 10. Inhibition zones of GSE (A), SBA-15-NH_2 (B), and SBA-15-NH_2@ GSE (C) on *E. coli*.

Table. 4. The Results of MIC and MBC for GSE and also SBA-15-NH_2@GSE using *S. aureus* and *E. coli*

Formulations	*S. aureus*		*E.coli*	
	MIC(mg/ml)	MBC(mg/ml)	MIC(mg/ml)	MBC(mg/ml)
GSE	2	8	4	16
SBA-15-NH_2@GSE	8	32	16	-

(-) no bactericidal effect was observed at used concentrations

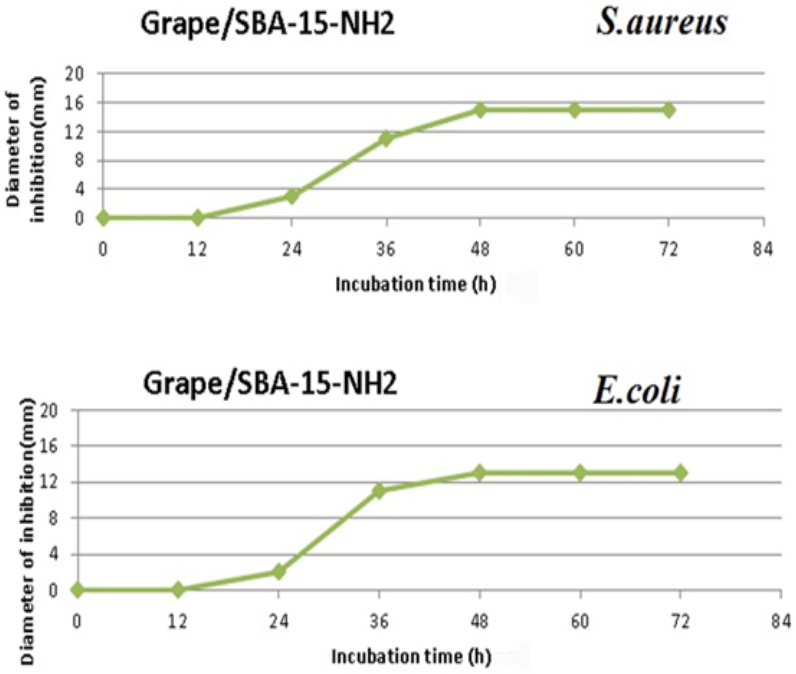

Fig. 11. The plot of growth zone inhibition for *S. aureus* (A) and *E. coli* (B) using SBA-15-NH_2@GSE.

References

Albayati T.M., Salih I.K., Alazzawi, H.F (2019) "Synthesis and characterization of a modified surface of SBA-15 mesoporous silica for a chloramphenicol drug delivery system." Heliyon 5: e02539.

Baek S, Singh R.K., Khanal D, Patel K.D, Lee E.J, Leong K.W, Chrzanowski W, Kim, H.W (2015) "Smart multifunctional drug delivery towards anticancer therapy harmonized in mesoporous nanoparticles." Nanoscale 7: 14191–14216.

Bagherzadeh M, Mahmoudi H, Amini M, Gautam S, Chae K.H. (2018) "SBA-15-supported copper (II) complex: An efficient heterogeneous catalyst for azide-alkyne cycloaddition in water." Scientia Iranica C 25(3): 1335-1343.

Brezoiu A.M, Prundeanu M, Berger D, Deaconu M, Matei C, Oprea O, Vasile E, Negreanu-Pîrjol T, Muntean D, Danciu C (2020) "Properties of Salvia officinalis L. and Thymus serpyllum L. Extracts Free and Embedded into Mesopores of Silica and Titania Nanomaterials." Nanomaterials 10: 820.

Chao C, Wen S, Xiaoli W, Yibing Wang, P.W (2018) "Rational design of curcumin loaded multifunctional mesoporous silica nanoparticles to enhance the cytotoxicity for targeted and controlled drug release." Mater. Sci. Eng. C 85: 88–96.

Divsar F, Isapour N, Kefayati H, Badiei A, Nezhadali A, Easapour S, Yadavi M (2014) "Fluorene functionalized nanoporous SBA-15 incorporated into carbon paste electrode for trace copper determination." RSC Adv. 22:59626-59631.

Doadrio J.C, Salinas A., Sánchez-Montero J (2015) "Vallet-Regí, M. Drug release from ordered mesoporous silicas." Curr. Pharm. Des. 21: 6213–6819.

Elbialy N.S, Aboushoushah S.F, Sofi B.F, Noorwali A.. (2020) "Multifunctional curcumin-loaded mesoporous silica nanoparticles for cancer chemoprevention and therapy." Microporous and Mesoporous Materials 291: 109540

Goscianska J, Olejnik A, Nowak I (2017) "APTES-functionalized mesoporous silica as a vehicle for antipyrine – adsorption and release studies, Colloids and Surfaces A." Physicochem. Eng. Aspects. 533:

187-196.

Holla G, Yeluri R, Munshi A.K (2012) "Evaluation of minimum inhibitory and minimum bactericidal concentration of nano-silver base inorganic anti-microbial agent (Novaron®) against *streptococcus mutans*." Contemp Clin Dent. 3(3): 288–293.

Jafari S, Derakhshankhah H, Alaei L, Fattahi A, Shiri Varnamkhasti B, Saboury A (2019) "Mesoporous silica nanoparticles for therapeutic/diagnostic applications." Biomedicine & Pharmacotherapy, 109: 1100-1111

Javanbakht M, Divsar F, Badiei A, Ganjali M.R, Norouzi P, Mohammadi Ziarani G, Chaloosi M, Abdi Jahangir A (2009) "Potentiometric detection of Mercury (II) ions using a carbon paste electrode modified with substituted thiourea-functionalized highly ordered nanoporous Silica." Anal. Sci. 25: 789-794

Javanbakht M, Divsar F, Badieid A, Fatollahi F, Khaniani Y, Ganjali M.R, Norouzi P, Chaloosi M, Mohammadi Ziarani G (2009) "Determination of picomolar silver concentrations by differential pulse anodic stripping voltammetry at a carbon paste electrode modified with phenylthiourea-functionalized high ordered nanoporous silica gel." Electrochimica. Acta., 54: 5381–5386.

Jayaprakasha G.K, Selvi T, Sakariah K.K (2003) "Antibacterial and Antioxidant Activities of Grape (Vitis vinifera) Seeds Extracts." Food Res. Int. 36: 117-122.

Li Y, Xu L, Bao Y, Cheng M, Wang H, Shan S, Yang R, Mao J (2018) "Hydrothermal synthesis of mesoporous carbons for adsorption of two alkaloids." J Porous Mater. 95-105.

Mellaerts R, Aerts C.A, Humbeeck J.V, Augustijns P, Mooter G.V, Martens J.A (2007) "Enhanced release of itraconazole from ordered mesoporous SBA-15 silica materials." Chem. Commun. 1375-1377.

Nahaei M.R, Kalejahi M, Rahbarfam P, Maleki Dizaj S, Lotfipour F (2016) "Evaluation the antibacterial effects of two commercial products of Eucalyptus globulus against common microbial causes of respiratory tract infections." Pharm. Sci. 22: 285-290.

Nassiri-Asl M, Hosseinzadeh H (2009) "Review of the pharmacological effects of Vitis vinifera (Grape) and its bioactive compounds." Phytother. Res. 23: 1197-1204.

Omara S.T (2017) "MIC and MBC of Honey and Gold Nanoparticles against methicillin-resistant (MRSA) and vancomycin-resistant (VRSA) coagulase-positive *S. aureus* isolated from contagious bovine clinical Mastitis." J. Genetic Engin. Biotech. 15: 219–230

Perumalla A.V.S, Hettiarachchy N.S. (2011) "Green tea and grape seed extracts —Potential applications in food safety and quality." Food Res. Int. 44: 827-839.

Shahriarinour M, Divsar F, Eskandari Z (2019) "Synthesis, characterization, and antibacterial activity of thymol loaded SBA-15 mesoporous silica nanoparticles." Inorganic and Nano-Metal Chemistry 49: 182-189.

Shahriarinour M, Rahimi F, Siahbani E, Kochakinejad R, Kaki S (2021) "A new electrochemical modified graphite pencil electrode developed for cholesterol assessing." J. Iranian Chem. Soc. 10(1): 1-13.

Shahriarinour M, Divsar F (2023). Release Kinetics and Antibacterial Property of Curcumin-Loaded Date Palm (*Phoenix dactylifera* L.) Pollen." Arab. J. Sci. Engin 48(6):7263-7272.

Shahriarinour M, Divsar F, Mehdipour A, Yousefftabar-Miri L, Barkhordri V (2023) "Antibacterial Properties of Cobalt Ferrite Magnetic Nanoparticles Loaded on Date Palm Pollen Against Multidrug-Resistant Bacteria." Arab. J. Sci. Engin 48(6):7315-7322

Song S.W, Hidajat K, Kawi S (2005) "Functionalized SBA-15 materials as carriers for controlled drug delivery: influence of surface properties on matrix-drug interactions." Langmuir 21: 9568-9575.

Xia E.Q, Deng G.F, Guo Y.J, Li H.B (2010) "Biological activities of polyphenols from grapes." Inter. J. Mol. Sci. 11: 622-646.

Yang Y, Yu C (2016) "Advances in silica based nanoparticles for targeted cancer therapy.." Nanomedicine 12: 317–332.

Yang C, Liu P, Ho Y, Chiu C, Chao K (2003) "Highly dispersed metal nanoparticles in functionalized SBA-15." Chem. Mater. 15: 275-280.

Yang K.N, Zhang C.Q, Wang W, Wang P.C, Zhou J.P, Liang X.J (2014) "pH-responsive mesoporous silica nanoparticles employed in controlled drug delivery systems for cancer treatment." Cancer Biol. Med. 11: 34–43.

Yarovaya L, Khunkitti W (2019) "Effect of grape seed extract as a sunscreen booster." Songklanakarin J. Sci. Technol. 41 (3): 708-715.

Zhao D.Y, Feng J.L, Huo Q.S (1998) "Triblock copolymer syntheses of mesoporous silica with periodic 50 to 300 angstrom pores." Science 279: 548-552.

Ziarani G.M, Badiei A, Mousavi S, Lashgari N, Shahbazi A (2012) ".Application of Amino-Functionalized SBA-15 Type Mesoporous Silica in One-Pot Synthesis of Spirooxindoles." Chin. J. Catal. 33:1832–1839.